Monthly Notices of the ROYAL ASTRONOMICAL SOCIETY
MNRAS **508,** 912–925 (2021) https://doi.org/10.1093/mnras/stab2532

Azimuthal propagation of star formation in nearby spiral galaxies: NGC 628, NGC 3726, and NGC 6946

F. Sakhibov,[1]★ A. S. Gusev [2] and C. Hemmerich[1]

[1]*University of Applied Sciences of Mittelhessen, Campus Friedberg, Department of Mathematics, Natural Sciences and Data Processing, Wilhelm-Leuschner-Straße 13, D-61169 Friedberg, Germany*
[2]*Sternberg Astronomical Institute, Lomonosov Moscow State University, Universitetsky pr. 13, 119234 Moscow, Russia*

Accepted 2021 August 26. Received 2021 August 8; in original form 2021 May 25

ABSTRACT

Star formation induced by a spiral shock wave, which in turn is generated by a spiral density wave, produces an azimuthal age gradient across the spiral arm, which has opposite signs on either side of the corotational resonance. An analysis of the spatial separation between young star clusters and nearby H II regions has made it possible to determine the position of the corotation radius in the galaxies studied. Fourier analysis of the gas velocity field in the same galaxies independently confirmed the corotation radius estimates obtained by the morphological method presented here.

Key words: galaxies: individual: NGC 628, NGC 3726, NGC 6946 – H II regions – open clusters and associations: general – galaxies: kinematics and dynamics – galaxies: spiral – galaxies: structure.

1 INTRODUCTION

The study of the distribution of star-formation locations in space and time provides an opportunity to understand the contribution of the various mechanisms governing star formation in spiral galaxies. One such mechanism is the large-scale spiral shock wave in the interstellar gas, which in turn is caused by a gravitational spiral density wave in the stellar disc. The possibility of the existence of a large-scale galactic shock wave was first shown in numerical calculations by Roberts (1969), and the physical characteristics were theoretically studied by Pikel'ner (1971), Shu et al. (1972), and Shu, Milione & Roberts (1973). The revealing of an age gradient for young stars across spiral arms is direct evidence of the existence of a galactic shock wave and the trigger nature of star formation in spiral arms. Such an age gradient of young stars has been found in the Sagittarius–Kiel arm of our Galaxy (Pavlovskaya & Suchkov 1984; Berdnikov 1987) and in the nearby galaxy M31 in the S4 arm (Efremov 1985). In the next-neighbouring spiral galaxy M33, Smirnov & Sakhibov (1981) have shown that the radial change in the annulus-averaged azimuthal offset between a subgroup of extremely young O stars and H II regions and a subgroup of relatively older B stars without ionized gas in star-forming regions at a galactocentric distance of ≈ 4.8 kpc changes sign. The authors interpreted this galactocentric distance of 4.8 kpc with its assumed distance of 720 kpc to the galaxy M33 as the radius of the corotation circle, within which the youngest subgroup of O stars and H II regions in the star-forming region lies closer to the inner (concave) side of the spiral arm. Vallée (2019) has found a spatial offset between the observed locations of Galactic radio masers from the centres of spiral arms, thus confirming the existence of an azimuthal age gradient in our Galaxy.

In other galaxies, the azimuthal gradient is much more difficult to detect due to the effects of light absorption and poor spatial resolution among other reasons. There are also a number of processes that can smear the azimuthal age gradient in the spiral arms. For example, star formation induced by a spiral shock wave can then stimulate a self-propagating star-formation process in the arms. This changes the age distribution of the stars in space and the age gradient across the arm becomes less evident. This may be one reason for the weakness or even absence of an age gradient in the external galaxies M83 (Talbot, Jensen & Dufur 1979), M33, M74 (NGC 628), and M81 (Guidoni, Messi & Natali 1981). Schweizer (1976) has described a scenario of colour behaviour in spiral arms if a shock caused by a spiral shock wave induces star formation. In this scenario, the bluer colour indices would be closer to the side of the spiral arm where the shock front is located, thereby reflecting the azimuthal gradient of ages across the spiral arm. However, photometric studies by Schweizer (1976) of the spiral arm structure of several galaxies have shown no age (colour) gradient, due to the fact that the increasing blueness towards the inner edge of the arm is compensated by increasing light absorption towards this edge. Using the stellar cluster catalogues of the galaxies NGC 1566, M51a, and NGC 628 from the Legacy ExtraGalactic UV Survey (LEGUS) programme, Shabani et al. (2018) studied cluster age gradients across the spiral arms in NGC 1566, M51a, and NGC 628. They confirmed the existence of an azimuthal age gradient across the spiral arms in NGC 1566 and found no offset in the azimuthal distribution of the studied samples of star clusters of different ages in galaxies M51a and NGC 628. In the same paper, Shabani et al. (2018) give a survey of studies of the azimuthal offset between different tracers in order to detect the sequence of stellar ages in spiral arms, as expected from stationary density-wave theory.

On the other hand, Puerari & Dottori (1997) investigated an azimuthal gradient of ages across the spiral arms through a comparison of the behaviour of the phase angle of the two-armed spiral in blue

★ E-mail: fsakhibov@yahoo.com

and infrared colours that pick out, respectively, young and older disc stellar populations. They found locations of the corotation radius in the galaxies NGC 1832 and NGC 7479 where an age gradient has opposite signs on either side of the corotation circle. The Puerari & Dottori (1997) method has been expanded and applied using more wavebands by a number of authors (see Sierra et al. 2015 and references therein). A comparison of the distribution of H II regions in the arms for the four grand-design spirals with the spatial distribution of the spiral density-wave isochrons also showed a self-consistent picture of the relationship between density-wave kinematics and star formation (Oey et al. 2003).

Star formation induced by a spiral shock can be a trigger for a stochastic self-propagating star-formation wave, caused by additional cloud compression in supernova explosions (Seiden 1985), or by the supersonic expansion of H II regions (ionization fronts) around hot OB stars (see Gusev & Shimanovskaya 2019 and references therein) and by the stellar wind. The Henize 206 nebula (Henize 1956)[1] is a prime example. The velocity of a stochastic self-propagating star-formation wave determines the magnitude of the spatial spread of stars of different ages in the regions of star formation, the so-called age gradient. Gusev & Shimanovskaya (2019) found a relation between the spatial separation S of young star clusters from the nearest H II regions and the age t ($U - B$ colour index) of star clusters on spatial scales from 40–500 pc and on time-scales from 10–300 Myr in five spiral galaxies: NGC 628, NGC 3184, NGC 3726, NGC 5585, and NGC 6946. Unlike star formation induced by a stationary spiral shock, a stochastic self-propagating star wave has no dedicated propagation direction and the age gradient caused by stochastic star formation makes it difficult to detect the azimuthal age gradient caused by a spiral shock. Gusev & Shimanovskaya (2019) showed that, contrary to the existence of a spiral structure, trends emerge in the galaxies that they studied, suggesting that in some cases spiral density waves are not the dominant mechanism. On the other hand, the global spiral patterns in grand-design galaxies, which is the case of NGC 628 studied here, certainly results from a spiral density wave. The contribution of the spiral shock wave to star formation should manifest itself through a characteristic change in the azimuthal component of the age gradient as a function of the distance from the galactic centre, or the azimuthal component of the spatial displacement of young star clusters with nearby H II regions. Therefore, the measurements of Gusev & Shimanovskaya (2019) can also be used to study star formation induced by a spiral shock wave.

The main aim of the current study is to reveal the correlation between the radial change in mean azimuthal offset between young star clusters from the nearest H II regions in star-forming regions and the corotation radius of the galaxy. This in turn shows that a galactic spiral shock wave is quite capable of stimulating a mechanism to trigger the gravitational collapse of gas clouds, leading to the formation of stars. A similar approach was first used by Smirnov & Sakhibov (1981), who studied the azimuthal offset between a subgroup of extremely young O stars and H II regions and a subgroup of relatively older B stars without ionized gas in star-forming regions in the nearby M33 galaxy.

The paper is structured as follows. In Section 2 we describe the method of the morphological analysis of spatial separations between a star cluster and the nearest H II region (hereafter called an SC–H IIR pair) in the galaxies studied. The data are discussed in Section 3 and the results presented in Section 4. Section 5 discusses the results and outstanding issues. Section 6 summarizes our conclusions.

[1] https://en.wikipedia.org/wiki/Henize206

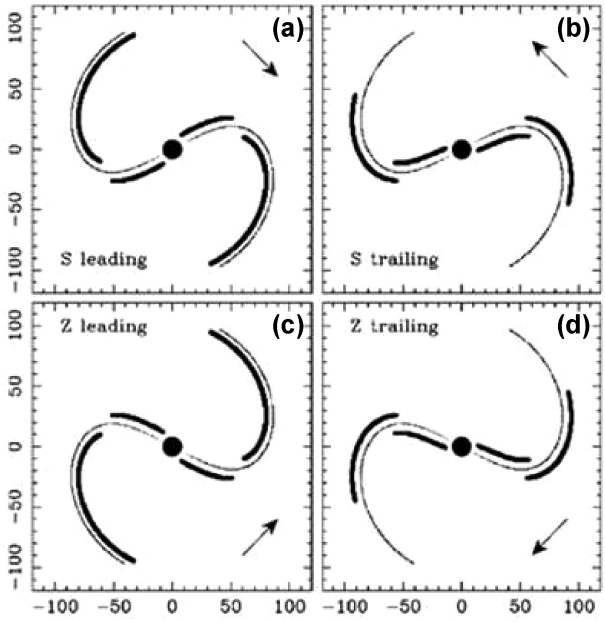

Figure 1. Taken from Puerari & Dottori (1997): Mutual location of the two-arm spiral pattern (thin line) and the stationary spiral shock wave in the interstellar gas (bold line). (a) The leading S-spiral, which rotates with the disc in a clockwise direction; (b) the trailing S-spiral that rotates counterclockwise to the disc; (c) the leading Z-spiral, which rotates with the disc in a clockwise direction; (d) the trailing Z-spiral that rotates counterclockwise to the disc.

2 THE METHOD

According to density-wave theory, a spiral-shaped region of gravitational disturbance in the homogeneous gravitational field of the disc, the so-called spiral pattern, rotates like a solid body and its rotation is characterized by some constant galactocentric distance-independent angular velocity Ω_P. The corotation radius R_C, where the rotation velocity of gas and stars in the disc coincides with the rotation speed of the spiral arms ($\Omega = \Omega_P$), is a fundamental parameter of density-wave theory that divides the Galactic disc into two regions: the region inside the corotation circle and the region outside the corotation circle. Within the region where the disc rotates faster than the spiral pattern ($\Omega > \Omega_P$), the stars and gas catch up with the gravitational spiral wave. In the outer region of the galaxy, where the disc rotates slower than the spiral pattern ($\Omega < \Omega_P$), the spiral wave catches up with the stars and gas. Thus stars and interstellar matter penetrate the arms in opposite directions when moving from the region inside the corotation circle to the region outside the corotation circle. Fig. 1, taken from Puerari & Dottori (1997), shows the mutual location of the two-arm spiral pattern (thin line) and the stationary spiral shock wave in the interstellar gas (bold line) for two possible directions of the pattern (S-shaped spiral and Z-shaped spiral; when viewed from Earth on the galactic plane, the S-shaped two-armed spiral galaxy is shaped like the letter 'S', while the Z-shaped two-armed spiral galaxy is shaped like the letter 'Z' and two possible directions of rotation, clockwise and counterclockwise, are visible on the celestial sphere). The galactocentric distance at which the shock front changes position relative to the side of the spiral pattern (from outside to inside or vice versa from inside to outside) is the corotation radius R_C at which the rotation velocity of

the gas and stars in the disc coincides with the rotation velocity of the spiral arms.

Our method consists of two independent approaches that help us to study the relationship between the spiral density wave and the star-formation process.

2.1 Defining the direction of azimuthal propagation of star formation in SC–H II R pairs and determining the corotation radius in a galaxy

In order to detect the impact of a spiral shock on the star-formation process propagation in star-formation complexes we calculated the azimuthal (tangential) component of the spatial offset between the photometric centres of star-formation regions in the galaxy images obtained with the B broad-band filter and Hα + [N II] narrow-band interference filter using the following formula:

$$\Delta_{\rm azimuth} = (\varphi_{\rm Cl} - \varphi_{\rm H\,II}) R_{\rm Cl} \quad (1)$$

where φ and R are the polar coordinates of the objects in the deprojected coordinate system. Lower indices indicate the type of object: 'Cl' for star cluster coordinates, 'H II' for H II region coordinates. To study the radial distribution of the azimuthal offset in SC–H II R pairs, the galaxy disc was divided into thin ring zones with width $\Delta R = 1$ kpc. For every ring zone, we computed a mean value for the azimuthal offset and considered its behaviour with changes in galactocentric distance.

If shock-induced star formation in the stellar density-wave scenario is real, one would expect a negative azimuthally averaged offset within the corotation circle for Z-spirals NGC 628 and NGC 6946 (the polar angle of the H II region $\varphi_{\rm H\,II}$ is greater than the polar angle of the star cluster $\varphi_{\rm Cl}$; see Fig. 1d and equation 1) and a positive azimuthally averaged offset in the case of the S-spiral NGC 3726 (the polar angle of the H II region $\varphi_{\rm H\,II}$ is less than the polar angle of the star cluster $\varphi_{\rm Cl}$; see Fig. 1b). Outside the corotation circle, the sign of the azimuthally averaged offset in the Z-spirals NGC 628 and NGC 6946 should be positive and that in the S-spiral NGC 3726 should be negative. These assumptions are valid if all three galaxies are trailing spirals. This means that the Z-spirals NGC 628 and NGC 6946 rotate clockwise and the S-spiral NGC 3726 rotates counterclockwise in the plane of the sky. In the case where the Z-spirals NGC 628 and NGC 6946 rotate counterclockwise and the S-spiral NGC 3726 rotates clockwise in the plane of the sky, we should expect a positive azimuthally averaged offset within the corotation circle for Z-spirals NGC 628 and NGC 6946 (see Fig. 1c and equation 1) and a negative azimuthally averaged offset in the case of the S-spiral NGC 3726 (Fig. 1a). This means that, by determining the sign of the azimuthally averaged offset inside and outside the corotation circle and taking into account the observed shape of the spirals (Z-shaped or S-shaped), we can determine the direction of the galaxy's rotation in the plane of the sky.

The galactocentric distance at which the azimuthally averaged offset changes sign can be interpreted, within the scenario of spiral density-wave shock-induced star formation, as the radius of corotational resonance.

2.2 Determining the corotation radius from the velocity field of the galaxy

To verify the determination of the corotation resonance radius via a change in the sign of the azimuthal offset inside and outside the corotation circle, we apply the kinematic method to determine the corotation radius in the galaxies studied. It is well known that the fundamental parameters of spiral density-wave theory, such as the corotation resonance position, may be determined by a Fourier analysis of the observed velocity field of the galaxy (Sakhibov & Smirnov 1987, 1989, 1990; Canzian 1993; Canzian & Allen 1997; Fridman et al. 2001a, b; Sakhibov et al. 2018; Zinchenko et al. 2019). We approximate the measured line-of-sight velocity $V_r^{\rm obs}(R, \varphi)$ at a given point (R, φ) of the disc, using a similar approach to that in Sakhibov et al. (2018) and Zinchenko et al. (2019):

$$\frac{V_r^{\rm obs}(R,\varphi)}{\sin i} = a_0 + a_1\cos(\varphi) + b_1\sin(\varphi) + \\ + a_2\cos(2\varphi) + b_2\sin(2\varphi) + a_3\cos(3\varphi) + b_3\sin(3\varphi) \quad (2)$$

where the angle i is the inclination of the galaxy and the Fourier coefficients a_0, a_1, b_1, a_2, b_2, a_3, and b_3 can be expressed in terms of the rotational velocity of the disc, the radial motion of the gas in the disc, and the streaming velocities of the gas in the spiral arms caused by the spiral density wave (see equation 7 in Zinchenko et al. 2019). The model described by equation (2) assumes that the 2D gas motion takes place in a thin disc whose thickness is negligibly small relative to the disc diameter. By taking into account the relation between the radial amplitude of the streaming velocity $\hat{u}$ and the frequency $\nu = m(\Omega_P - \Omega)/\kappa$ of the spiral pattern

$$\hat{u} = A\nu \quad (3)$$

and the relation between the tangential amplitude $\hat{v}$ of the streaming velocity and the epicyclic frequency κ

$$\hat{v} = A\kappa/(2\Omega) \quad (4)$$

and using formulas for the Fourier coefficients (equation 7 in Zinchenko et al. 2019), we obtain a criterion for determining the corotation radius from the relations between the Fourier coefficients found:

$$\Big(\Omega_{P,1} - \Omega\Big)h \propto (a_2^2 + b_2^2)^2 \sin^2\Big(\cot\mu_1 \ln(R/R_{01}) - \mu_1\Big) - (a_0 - V_{\rm sys})^2, \quad (5)$$

$$\Big(\Omega_{P,2} - \Omega\Big)h \propto (a_3^2 + b_3^2)^2 \cos^2\Big(2\cot\mu_2 \ln(R/R_{02}) - \mu_2\Big) - (b_1 - V_R)^2, \quad (6)$$

where A in equations (3) and (4) is a scaling coefficient composed of physical factors (Shu et al. 1973), the quantities $V_{\rm sys}$, μ_1, and R_{01} in equation (5) mean the systemic velocity of the galaxy, the pitch angle, and scaling factor for the first mode ($m = 1$), and the quantities V_R, μ_2, and R_{02} in equation (6) stand for the the radial gas flow velocity in the galactic disc, the pitch angle, and the scaling factor for the second mode ($m = 2$) of a spiral density wave, respectively. Factor h in equations (5) and (6) is equal to $+1$ for S-shaped spirals and -1 for Z-shaped spirals. Pitch angles μ_1 and μ_2 are also determined from the radial change in Fourier coefficients using the following formulas:

$$\mu_1 = \arctan\left(\frac{h\ln(R_{n+1}/R_n)}{\arctan\left(a_2(R_{n+1})/b_2(R_{n+1}) - a_2(R_n)/b_2(R_n)\right)}\right), \quad (7)$$

$$\mu_2 = \arctan\left(\frac{2h\ln(R_{n+1}/R_n)}{\arctan\left(a_3(R_{n+1})/b_3(R_{n+1}) - a_3(R_n)/b_3(R_n)\right)}\right), \quad (8)$$

where $a_2(R_n)$, $b_2(R_n)$, $a_3(R_n)$, and $b_3(R_n)$ mean the Fourier coefficient found in the nth ring zone. The relation in equation (5) expresses the criterion for determining the corotation resonance for the first mode ($m = 1$) of the density wave. The galactocentric distance at which the right-hand side of equation (5) changes sign is the radius of corotation of the spiral pattern for the first mode ($m = 1$). The relation in equation (6) expresses the criterion for determining the

corotation resonance for the second mode ($m = 2$) of the density wave. The galactocentric distance at which the right-hand side of expression (6) changes sign is the radius of corotation of the spiral pattern for the second mode ($m = 2$).

We briefly make some remarks on the definition of Fourier coefficients in the present study.

(i) Since all the galaxies studied in the current paper have a bar or bar-like structure, we confined our analysis of the velocity field to the outer region of the disc, where no material flows along the bar and rotates with it, and the effect of the bar is weak or negligible.

(ii) Coefficient $b_1(R)$ in equation (2) comprises generally radial outflow/inflow motion $V_R(R)$ and a radial component of the velocity perturbations from spirals:

$$b_1(R) = V_R(R) + A(R)\cos\Big(\cot\mu_2 \ln(R/R_{02}) - \mu_2\Big). \quad (9)$$

$V_R(R)$ is in general also a function of R and cannot be easily disentangled from the impact of the streaming velocities in spirals. To account for the impact of V_R on the b_1 coefficient, we used the modernized approximation method described in our earlier paper (Sakhibov & Smirnov 1987). In the current approach, unlike the earlier one, the pitch angle was determined independently using equation (8).

3 THE DATA

To find a systematic variation in the azimuthal offset in SC–H II R pairs as a function of galactocentric distance, we used the coordinate pairs presented in Gusev & Shimanovskaya (2019). We selected three galaxies, NGC 628, NGC 3726, and NGC 6946, with a representative sample of SC–H II R pairs (see Table 1) from the sample of five nearby galaxies studied in Gusev & Shimanovskaya (2019). Photometric *UBVRI* and H α + [N II] observations taken with the 1.5 m telescope at Mt Maidanak Observatory in Uzbekistan and procedures for the identification and preliminary selection of star-forming regions in B and H α images of galaxies using the SExtractor[2] program are described in detail in Gusev et al. (2018). The plate coordinates of all objects (star clusters in B images and H II regions in H α images) were recalculated in deprojected ones, using corresponding position angles and inclinations of galaxies. As objects of study, we used the 'stellar cluster–H II region' pairs selected earlier in Gusev & Shimanovskaya (2019). To avoid random SC–H II R pairs, the age of clusters among the candidates was controlled using the relationship between the $U - B$ colour index and the cluster age predicted by stellar population evolution models. For detailed criteria for the selection procedure of chosen pairs, see Gusev & Shimanovskaya (2019).

The final sample includes 503 'stellar cluster–H II region' pairs in NGC 628, 254 pairs in NGC 3726, and 577 pairs in NGC 6946. Examples of selected pairs are illustrated in fig. 6 in Gusev & Shimanovskaya (2019). An example of the full sample of identified and finally selected star clusters and H II regions in NGC 628 used in the current paper can be seen in fig. 7 in Gusev & Shimanovskaya (2019). The global parameters of the selected galaxies are compiled in Table 1.

Fig. 2 shows, as an example, a map of the distribution of the studied SC–H II R pairs in NGC 628.

In Fig. 3 we compare the azimuthal offsets in 62 SC–H II R pairs from this study with the azimuthal offsets in 62 SC–H II R pairs observed with the *Hubble Space Telescope* (*HST*). We have identified our H II regions with the H II regions observed with SITELLE at the Canada–France–Hawaii Telescope (CFHT) (Rousseau-Nepton et al. 2018)[3] and our stellar clusters with clusters extracted from the Legacy ExtraGalactic UV Survey with *HST* (LEGUS) star cluster catalogue (Adamo et al. 2017).[4] While a sample of 4285 H II regions from Rousseau-Nepton et al. (2018) covers the whole galaxy, a sample of star clusters from LEGUS covers only part of the disc of NGC 628. The area of the disc covered by SC–H II R pairs from the *HST* observations comprises 223 of our pairs out of a total of 503 SC–H II R pairs considered in the current study. Of these 223 SC–H II R pairs, we identified 62 pairs with pairs observed by *HST* with compatible cluster age estimates. Fig. 3 shows that our H II region–cluster pairings remain valid when observed with the much higher angular resolution provided by *HST*.

To apply the kinematic method to determine the corotation radius, we used published velocity fields in the galaxies studied.

The spiral galaxy NGC 628 is one of the galaxies whose kinematics has been studied in detail. Shostak & van der Kruit (1984) constructed a two-dimensional field of H I line-of-sight velocities for the inner optically visible part of the galaxy using the aperture synthesis method. Kamphuis & Briggs (1992) extended this field to the outer part of the galaxy, which is detectable in the radio range. These observations showed that the kinematics of the gas in the optical part of the galaxy corresponds to a flat differentially rotating disc. The velocity field in the outer non-optical part of the disc deviates from the model for a flat differentially rotating disc and exhibits a complex irregular structure. Kamphuis & Briggs (1992) give a detailed discussion of peculiar motions in the outer non-optical part of NGC 628. To exploit criteria (5) and (6) for determining the radius of corotation, we performed a Fourier analysis of the two-dimensional H I velocity field presented in Shostak & van der Kruit (1984), which has a velocity resolution of 5 km s^{-1}. A detailed discussion of the corresponding Westerbork Synthesis Radio Telescope (WSRT) observations can be found in Shostak & van der Kruit (1984). We did not use the velocity field of the H II regions in galaxy NGC 628, obtained by Sanchez et al. (2011) using integral field spectroscopy (IFS), because the observations cover a field of ~6 arcmin in diameter and do not cover the outer parts of the spiral pattern of NGC 628. In addition, the number of points in the field of the disc, where light-of-sight velocities were measured, is lower than 300 and does not provide sufficient accuracy for the calculated parameters.

The observational data of H I line-of-sight velocities in NGC 3726 are also from the 21 cm line synthesis imaging with the Westerbork Synthesis Radio Telescope (Verheijen & Sancisi 2001).

The spiral galaxy NGC 6946 is also a galaxy for which there is a good data base for a detailed study of kinematics. Suffice it to say that two-dimensional line-of-sight velocity fields of neutral hydrogen were constructed for this galaxy as early as 1973 using the aperture synthesis method (Rogstad & Shostak 1973), later repeated by observations of ionized hydrogen (Bonnare et al. 1988) and Westerbork H I line observations of Carignan et al. (1990). The authors of these observations studied the mass distribution in NGC 6946 and constructed rotation curves. The perturbed velocities in the disc of the galaxy have not been studied further. The

[2] http://sextractor.sourceforge.net/

[3] https://academic.oup.com/mnras/article/477/3/4152/4898083#supplementary-data

[4] https://archive.stsci.edu/prepds/legus/dataproducts-public.html

Table 1. The galaxy sample.

Galaxy	Number of Cl–H II pairs	Type	B_t	M_B^a [mag]	Inclination [degree]	PA [degree]	R_{25}^b [arcmin]	R_{25}^b [kpc]	D [Mpc]	$A(B)_{\rm Gal}$ [mag]	$A(B)_{\rm in}$ [mag]
1	2	3	4	5	6	7	8	9	10	11	12
NGC 628	503	SA(s)c	9.70	−20.72	7	25	5.23	11.0	7.2	0.254	0.04
NGC 3726	254	SAB(r)c	10.31	−20.72	49	16	2.62	10.9	14.3	0.060	0.30
NGC 6946	577	SAB(rs)cd	9.75	−20.68	31	62	7.74	13.3	5.9	1.241	0.04

Notes. [a]Absolute magnitude of a galaxy corrected for Galactic extinction and inclination effects.
[b]Radius of a galaxy at the isophotal level 25 mag arcsec^{-2} in the B band corrected for Galactic extinction and inclination effects.

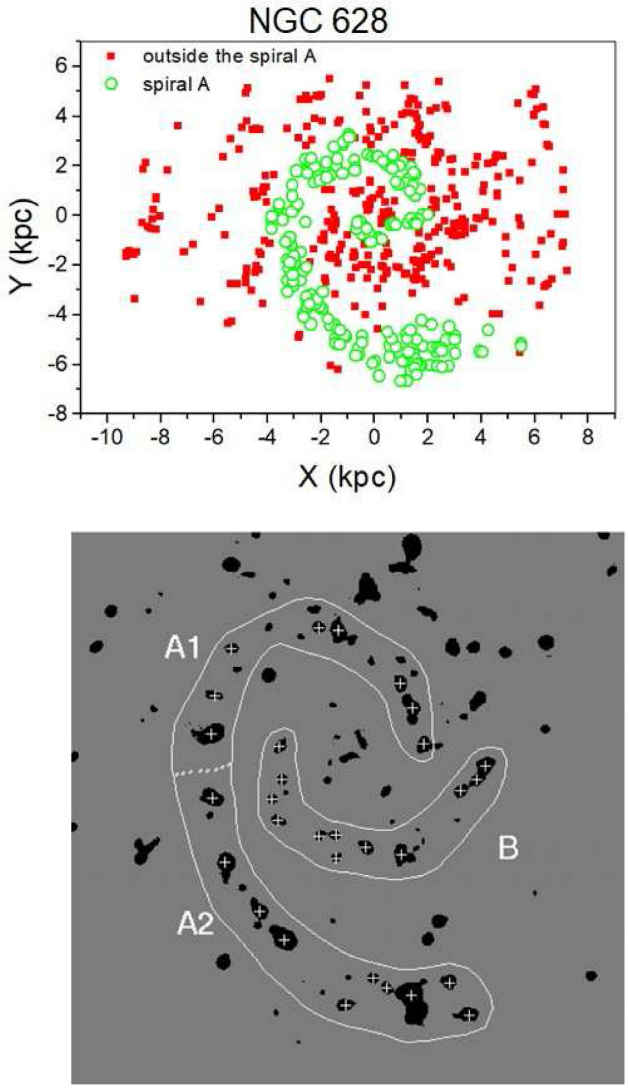

Figure 2. Map of the distribution of 503 SC–H IIR pairs in NGC 628. The upper panel shows the 324 SC–H IIR pairs outside spiral arm A as filled squares; the 179 SC–H IIR pairs in spiral arm A are shown as open circles. The bottom panel shows the boundaries of spiral A, whose peculiar properties were studied in our earlier article (Gusev, Egorov & Sakhibov 2014).

results of measurements of the line-of-sight velocities of ionized hydrogen were unfortunately not given in Bonnare et al. (1988), and are now lost. To exploit criteria (5) and (6) for determining the radius of corotation, we calculated the radial variation of Fourier coefficients in the disc of NGC 6946 using the velocity field obtained by Carignan et al. (1990). Observations made with

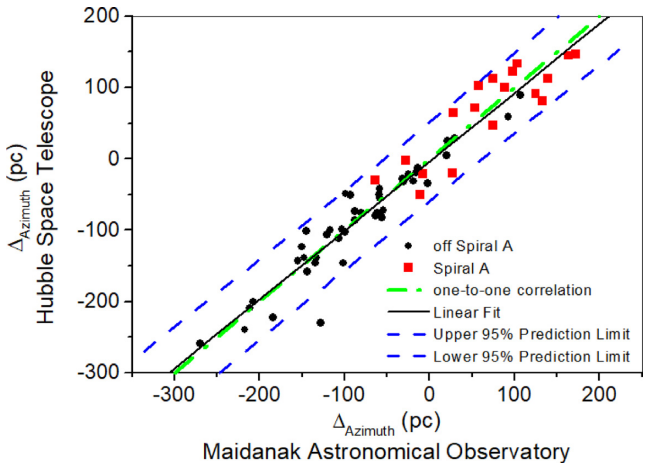

Figure 3. Comparison between our and the reference azimuthal offsets in SC–H IIR pairs in NGC 628 from the *HST* observations. SC–H IIR pairs outside spiral arm A are shown as black circles, the SC–H IIR pairs in spiral arm A are shown as red squares. The solid line is the linear fit, computed for azimuthal offsets in SC–H IIR pairs (circles and squares). Dashed lines are upper and lower 95 per cent prediction limits of the linear fit. The dot–dashed line is a one-to-one correlation and actually corresponds to the linear fit.

the WSRT are discussed in detail by the authors (Carignan et al. 1990).

4 RESULTS

4.1 NGC 628

A comparative analysis of the 30 brightest UV star-forming regions in the A and B arms (see Fig. 2) in NGC 628, carried out in our earlier paper (Gusev et al. 2014), shows that the star-forming regions in spiral arm A are systematically brighter in the UV and the Hα line, larger in size, higher in star-formation rate, lower in metallicity, and relatively lower in age than the brightest star-forming regions in the B arm. Given this result, we have examined the behaviour of the mean azimuthal offset in the ring zones as a function of galactocentric distance for three samples of objects. First, we plotted the average azimuthal offset versus galactocentric distance for all 503 SC–H IIR pairs. A separate dependence was then plotted for the 179 SC–H IIR pairs populating peculiar arm A, and finally a dependence for the remaining 324 SC–H IIR pairs outside arm A.

Fig. 4 shows the change in the azimuthally averaged offset, calculated from equation (1), in the annulus with galactocentric radius R. Panel (a) shows the radial change of the azimuthally averaged offset in the annulus calculated for all 503 SC–H IIR pairs in NGC 628, panel (b) shows the radial change of the azimuthally

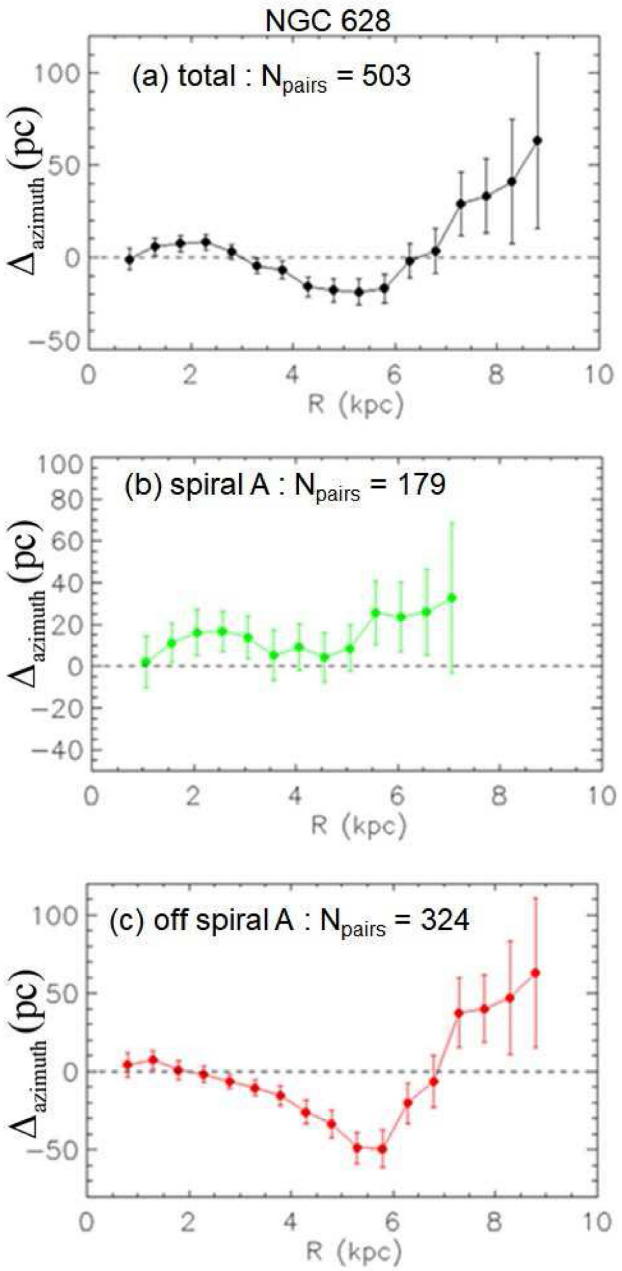

Figure 4. Variation of the mean azimuthal offset in the annulus with the galactocentric radius R. (a) The radial change in azimuthally averaged offset in the annulus calculated for all 503 SC–H IIR pairs in NGC 628; (b) the radial change in azimuthally averaged offset calculated for 179 SC–H IIR pairs in spiral A; (c) the radial change in azimuthally averaged offset calculated for 324 SC–H IIR pairs outside spiral A.

averaged offset calculated for 179 SC–H IIR pairs in spiral A shown in Fig. 2 as open circles, and panel (c) shows the radial change of the azimuthally averaged offset calculated for 324 SC–H IIR pairs outside spiral A. Fig. 4 shows that the curve calculated for all SC–H IIR pairs (panel a) is the sum of the curves calculated separately for SC–H IIR pairs in spiral arm A (panel b) and outside arm A (panel c).

Consider first the radial course of the average azimuthal offset calculated for pairs located outside spiral arm A (Fig. 4c). Fig. 4(c) shows that the azimuthally averaged offset, calculated for SC–H IIR pairs located outside spiral arm A, changes with galactocentric distance as follows:

(i) in the central region of the disc ($R < 2$ kpc) with a possibly bar-like structure (Seigar 2002), the mean azimuthal offset is not evident;

(ii) between galactocentric distances of 2 kpc and about 7 kpc, the negative azimuthally averaged offset grows from zero to peak at $R \approx 5.5$ kpc, then drops to zero and changes from negative to positive at galactocentric distance $R \approx 7$ kpc;

(iii) at galactocentric distances greater than 7 kpc, the positive sign of the mean azimuthal offset is held, and its magnitude increases with distance.

The negative sign of the azimuthal offset calculated with equation (1) in the case of the Z-spiral NGC 628 means that, in the range of galactocentric distances from 2–7 kpc, extremely young stars surrounded by regions of ionized hydrogen are on average closer to the inner edge of the spiral arm in SC–H IIR pairs than relatively old star clusters without ionized gas. The positive sign of the azimuthal offset at galactocentric distances greater than 7 kpc means that extremely young stars, surrounded by regions of ionized hydrogen, are on average closer to the outer edge of the spiral arm within the SC–H IIR pairs than relatively old star clusters without ionized hydrogen. This also means that, inside a circle with a radius of 7 kpc, the matter in the galactic disc rotates faster than the spiral pattern, and outside this circle, the spiral pattern rotates faster than the matter in the disc. That is, the substance in the disc of NGC 628 rotates in a clockwise direction. The circle itself with radius $R = 7.0 \pm 1.0$ kpc is the so-called corotation circle, where the rotational velocity of the matter in the disc coincides with the rotational velocity of the spiral pattern.

The radial variation of criterion (6) (case $m = 2$), calculated using Fourier coefficients derived from analysis of the velocity field of NGC 628, shows that at a distance $R_{C,\,m=2} = 6.2 \pm 1.0$ kpc the spiral pattern rotation speed is equal to that of the disc (Fig. 5). We designate the corotation radius obtained using the kinematic method as follows: $R_{C,\,m=2}$, where the index '$m = 2$' indicates the second mode of the spiral density wave.

Next, consider the radial variation of the azimuthally averaged offset in spiral arm A. Fig. 4(c) shows that the average azimuthal offset, calculated for SC–H IIR pairs located in spiral arm A, has a positive sign all along the arm in the interval of galactocentric distances from 1–7 kpc. The positive sign of the mean azimuthal offset over the whole spiral arm A from $R = 1$–7 kpc means that young populations of stars, surrounded by regions of ionized hydrogen, are on average closer to the outer edge of spiral arm A within the SC–H IIR pairs than relatively old star clusters without ionized gas. Does this mean that spiral arm A rotates faster than the matter in the disc over its entire extension? If so, how can this be?

It can be expected that at least two modes of the spiral density wave are realized in NGC 628: the first mode ($m = 1$) and the second mode ($m = 2$). The concurrent realization of the first and second modes permits the existence of two independent spiral pattern systems with different pitch angles (geometry) and rotational rates. The concurrent existence of a single-arm and a double-arm spiral structure can manifest itself in differences in the degree of development of the spiral arms, in the asymmetry of the grand design (see Elmegreen, Elmegreen & Montenegro 1992 and references therein). The one-arm structure as spiral A is clearly visible in the image of the asymmetric structure obtained from the computer-enhanced image of galaxy NGC 628 (see the middle right-hand panel in fig. 1d in Elmegreen et al. 1992). Assuming that the azimuthal offset in SC–H IIR pairs is

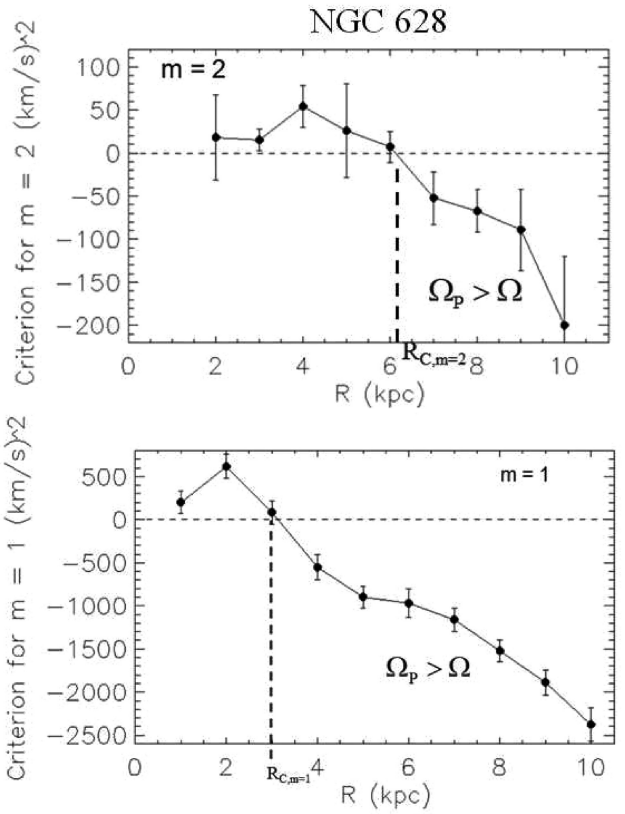

Figure 5. Radial variation of the quantity proportional to the difference between the angular velocity of the spiral pattern and the angular velocity of the substance in the disc, computed using Fourier coefficients derived from an analysis of the velocity field of the galaxy NGC 628 (upper panel: case $m = 2$, bottom panel: case $m = 1$).

initiated by a spiral shock, and assuming that the peculiar arm A is driven by the first mode of the spiral density wave, one would expect the resonance for this mode to occur at a smaller galactocentric distance, thereby providing a larger rotation rate for spiral A.

The radial variation of the criterion for the first mode (equation 5), calculated using Fourier coefficients derived from analysis of the velocity field of NGC 628, shows that at distance $R_{C,\,m=1} = 3 \pm 1$ kpc the spiral pattern rotation velocity is equal to that of the disc (see Fig. 5, bottom panel). The index '$m = 1$' indicates the first mode of the spiral density wave. This means that, outside the circle with a radius of 3 kpc, the peculiar spiral arm A, presumably caused by the first mode of the spiral density wave, rotates faster than the matter in the disc. That is, the spiral shock front is located on the outer side of spiral A and the sign of the azimuthal offset calculated by equation (1) must be positive. Fig. 4(b) shows this.

The radial variation of averaged azimuthal offset computed for all 503 pairs (Fig. 4a), including the pairs inhabiting spiral arm A, shows that there are two radii where the averaged azimuthal offset in pairs changes sign. The outer corotation radius at 6.3 kpc is compatible with a resonance detected for the second mode ($m = 2$) of the spiral density wave (Fig. 5, upper panel) and with corotation radius $R_{C,\,outer} = 7 \pm 1$ kpc derived from radial change of averaged azimuthal offset computed for 324 pairs outside spiral A. The inner corotation radius at $R_{C,\,inner} = 3 \pm 1$ kpc is compatible with a resonance detected for the first mode ($m = 1$) of the spiral density wave (Fig. 5, lower panel), with a minimum close to zero (zero lies in the error interval) of averaged azimuthal offset computed for 179 pairs in spiral A

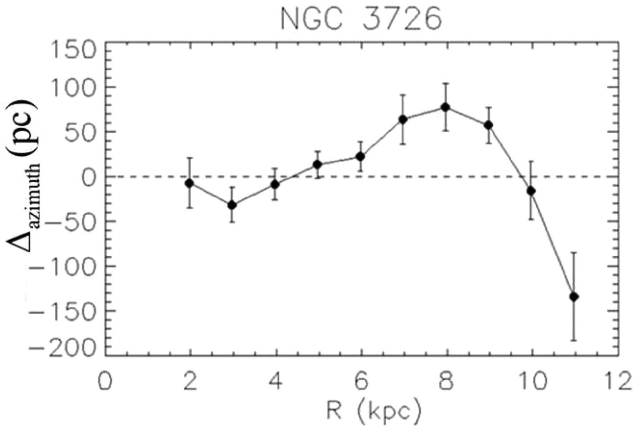

Figure 6. Radial change in azimuthally averaged offset in the annulus calculated for 254 SC–H IIR pairs in NGC 3726.

(Fig. 4b), and with an inner corotation radius of averaged azimuthal offset computed for 324 pairs outside spiral A (Fig. 4c). The positive sign of the azimuthal offset in arm A inside the corotation circle of the first mode will be discussed below in Section 5.

4.2 NGC 3726

Fig. 6 shows the radial change in azimuthally averaged offset in the annulus calculated for 254 SC–H IIR pairs in the barred galaxy NGC 3726. There are three cases of a sign change in the azimuthal offset in NGC 3726 at galactocentric distances of about $R_{C1} \approx 2$ kpc, $R_{C2} \approx 4.4$ kpc, and $R_{C3} \approx 9.8$ kpc. The innermost resonance appears to be associated with an inner mass concentration of the bar and coincides with the first resonance detected by Font et al. (2011, 2014) using the Font–Beckman (FB) method from residual velocity field analysis and by Buta & Zhang (2009) using the potential-density phase-shift method, while the two outer resonances are features of the disc. Starting at the galactocentric distance $R = 4.5$ kpc, outside the region inhabited by the bar, and up to about 9.8 kpc, the positive azimuthally averaged offset increases from zero to peak at $R \approx 8$ kpc then drops to zero and changes from positive to negative at galactocentric distance $R \approx 9.8$ kpc. The positive sign of the azimuthal offset computed with equation (1) in the case of the S-shaped spiral NGC 3726 means that, in the interval of galactocentric distances from 4.5–9.8 kpc, extremely young stars surrounded by regions of ionized hydrogen are on average in the SC–H IIR pairs closer to the inner edge of the spiral arm than relatively old star clusters without ionized gas.

The negative sign of the azimuthally averaged offset at galactocentric distances greater than 9.8 kpc means that extremely young stars, surrounded by regions of ionized hydrogen, are closer to the outer edge of the spiral arm within the SC–H IIR pairs than relatively old star clusters without ionized hydrogen. This also means that, in the interval of galactocentric distances from 4.5–9.8 kpc, the matter in the galactic disc rotates faster than the spiral pattern and, outside this circle, the spiral pattern rotates faster than the matter in the disc. That is, the substance in the disc of NGC 3726 rotates in a counterclockwise direction. The circle itself with radius $R_{C3} = 9.8 \pm 1.0$ kpc is the corotation circle, where the rotational velocity of the matter in the disc coincides with the rotational velocity of the spiral pattern.

The radial variation of criterion (6) (case $m = 2$), calculated using Fourier coefficients derived from analysis of the velocity field of NGC 3726, shows that at distance $R_{C,\,m=2} = 9.3 \pm 1.0$ kpc the spiral

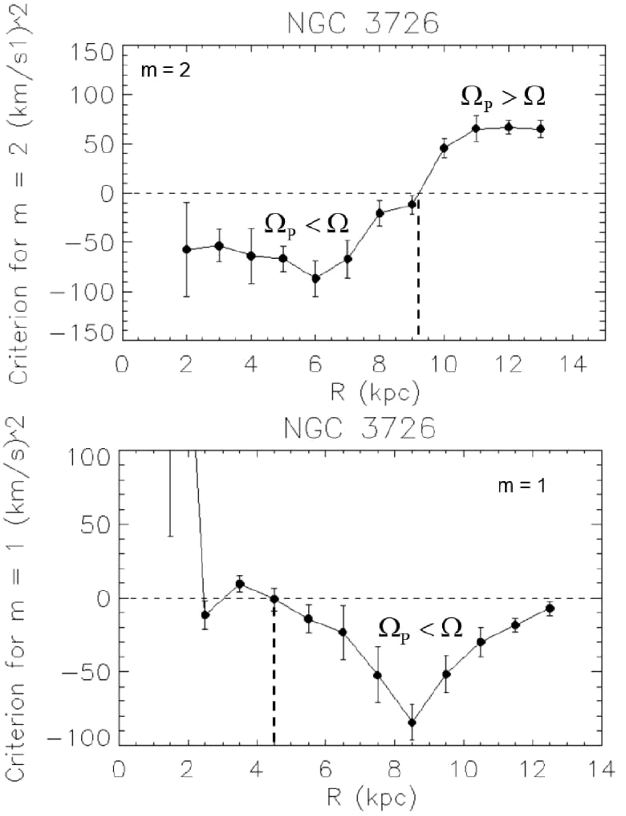

Figure 7. Radial variation of the quantity proportional to the difference between the angular velocity of the spiral pattern and the angular velocity of the substance in the disc, computed using Fourier coefficients derived from an analysis of the velocity field of the galaxy NGC 3726 (upper panel: case $m = 2$, bottom panel: case $m = 1$).

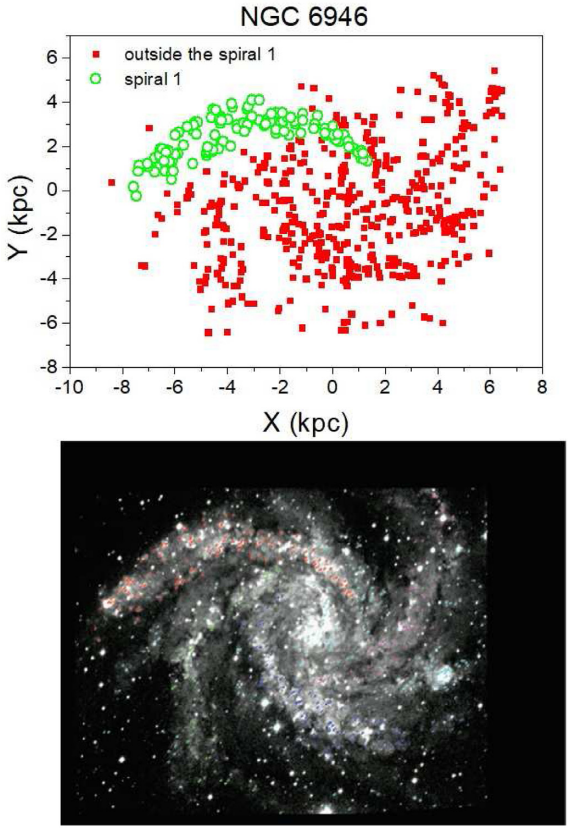

Figure 8. Map of the distribution of SC–H IIR pairs in NGC 6946. The upper panel shows the SC–H IIR pairs outside spiral arm 1 as filled squares; the SC–H IIR pairs in spiral arm A are shown as open circles. The bottom panel shows a face-on *B* image of NGC 6946 from our earlier papers (see Gusev et al. 2015, 2016).

pattern speed is equal to that of the disc (upper panel in Fig. 7). The radial variation of criterion (5) (case $m = 1$), shows that at distance $R_{C,\,m=1} = 4.5 \pm 1.0$ kpc the spiral pattern speed is equal to that of the disc (bottom panel in Fig. 7). Note that Font et al. (2014) also classify NGC 3726 as a system with two coupling spiral patterns.

4.3 NGC 6946

According to Arp's classification (Arp 1966), NGC 6946 belongs to the class of 'spiral galaxies with one heavy arm'. The spiral arms in these galaxies have an asymmetrical position, so one of them is distinguished by its brightness. Therefore, we examined the behaviour of the mean azimuthal offset in the ring zones as a function of galactocentric distance for three samples of objects. First, we plotted the azimuthally averaged offset versus galactocentric distance for all 577 SC–H IIR pairs. Then we plotted a separate dependence for the 118 SC–H IIR pairs populating the 'heavy arm', and finally a dependence for the remaining 459 SC–H IIR pairs outside the 'heavy arm'. Hereinafter we will refer to the 'heavy arm' as 'spiral arm 1'. SC–H IIR pairs populating spiral arm 1 in NGS 6946 are shown on the map (Fig. 8, top panel) with open circles.

Fig. 9 shows the change in the azimuthally averaged offset, calculated from equation (1), in the annulus with galactocentric radius *R*. Panel (a) shows the radial change in azimuthally averaged offset in the annulus calculated for all 577 SC–H IIR pairs in NGC 6946,;panel (b) shows the radial change of the azimuthally averaged offset, calculated for 118 SC–H IIR pairs in 'heavy' spiral 1, shown in Fig. 8 as open circles; and panel (c) shows the radial change of the azimuthally averaged offset calculated for 459 SC–H IIR pairs outside spiral 1. Fig. 9 shows that the curve calculated for all SC–H IIR pairs (panel a) is the sum of the curves calculated separately for SC–H IIR pairs in spiral arm 1 (panel b) and outside arm 1 (panel c).

Consider first the radial course of the mean azimuthal offset calculated for pairs located outside the 'heavy' spiral arm 1 (Fig. 9c). Fig. 9(c) shows that the average azimuthal offset, calculated for SC–H IIR pairs located outside spiral arm 1, changes with the change in galactocentric distance as follows:

(i) between galactocentric distances of 1 kpc and about 4.5 kpc, the negative azimuthally averaged offset grows from zero to peak at $R \approx 3$ kpc, then drops to zero and changes from negative to positive at galactocentric distance $R \approx 4.5$ kpc;

(ii) at galactocentric distances greater than 5 kpc, the positive sign of the mean azimuthal offset is held, and its magnitude increases with distance.

The negative sign of the azimuthal offset calculated with equation (1) in the case of the Z-shaped spiral NGC 6946 means that, in the interval of galactocentric distances from 1–4.5 kpc, extremely young stars surrounded by regions of ionized hydrogen are closer to the inner edge of the spiral arm within the SC–H IIR pairs than relatively old star clusters without ionized hydrogen.

The positive sign of the mean azimuthal offset at galactocentric distances greater than 5 kpc means that extremely young stars,

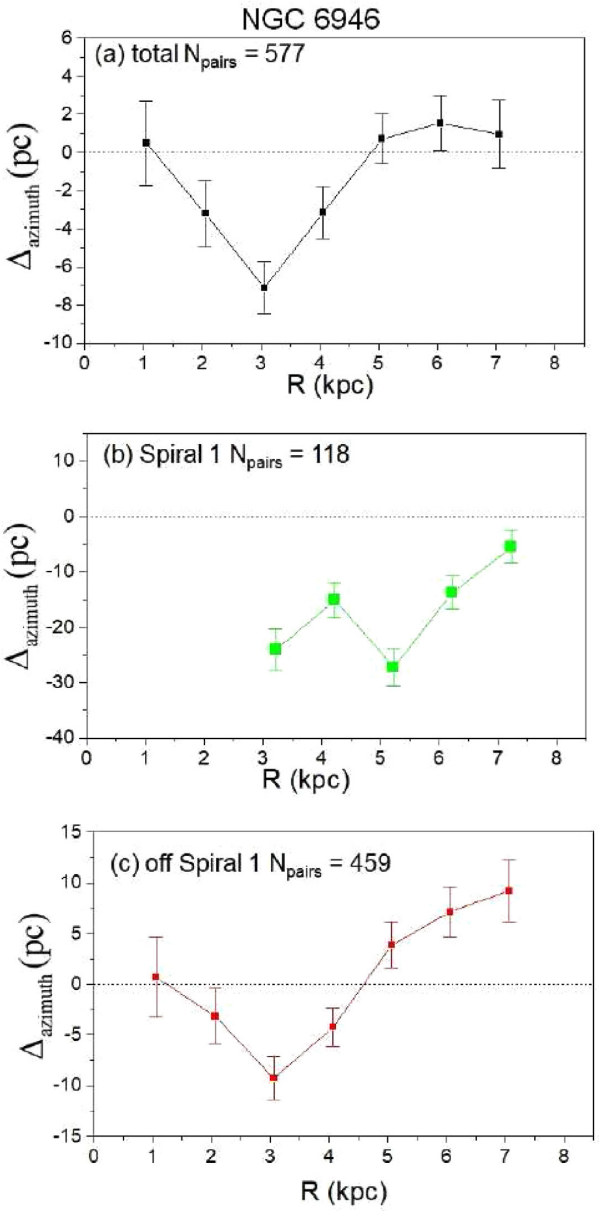

Figure 9. Variation of the mean azimuthally averaged offset in the annulus with the galactocentric radius R. (a) The radial change in azimuthally averaged offset in the annulus calculated for all 577 SC–H II R pairs in NGC 6946; (b) the radial change in azimuthally averaged offset calculated for 118 SC–H II R pairs in spiral 1 ('heavy arm'); (c) the radial change in azimuthally averaged offset calculated for 459 SC–H II R pairs outside spiral 1.

surrounded by regions of ionized hydrogen, are closer to the outer edge of the spiral arm within the SC–H II R pairs than relatively old star clusters without ionized hydrogen. This also means that, inside a circle with a radius of 4.5 kpc, the matter in the galactic disc rotates faster than the spiral pattern and, outside this circle, the spiral pattern rotates faster than the matter in the disc. That is, the substance in the disc of NGC 6946 rotates in a clockwise direction. The circle itself with radius $R = 4.5 \pm 1.0$ kpc is the so-called corotation circle, where the rotational velocity of the matter in the disc coincides with the rotational velocity of the spiral pattern.

The radial variation of criterion (6) (case $m = 2$), calculated using Fourier coefficients derived from analysis of the velocity field of

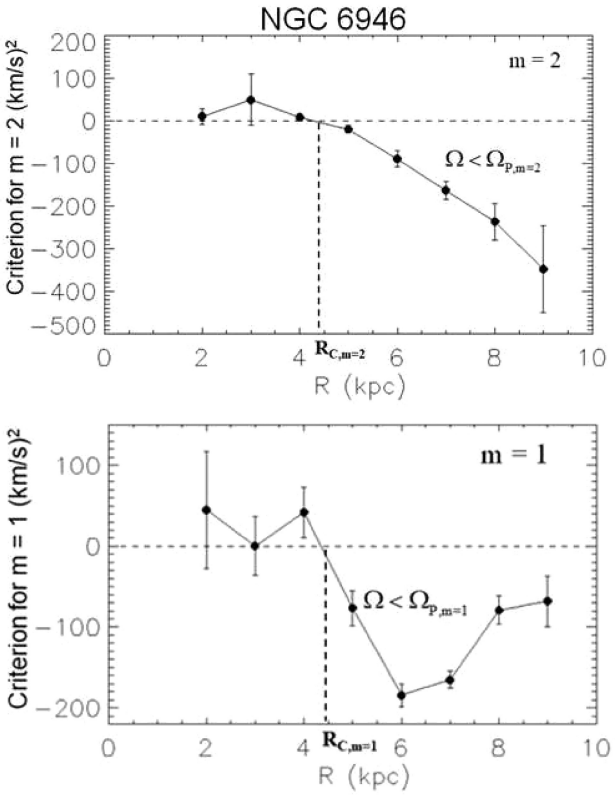

Figure 10. Radial variation of the quantity proportional to the difference between the angular velocity of the spiral pattern and the angular velocity of the substance in the disc, computed using Fourier coefficients derived from an analysis of the velocity field of the galaxy NGC 6946 (upper panel: case $m = 2$, bottom panel: case $m = 1$).

NGC 6946, shows that at distance $R = 4.4 \pm 1.0$ kpc the spiral pattern rotation velocity is equal to that of the disc (see Fig. 10).

Next, consider the radial variation of the mean azimuthal offset in the heavy spiral arm 1. Fig. 9(b) shows that the average azimuthal offset, calculated for SC–H II R pairs located in spiral arm 1, has a negative sign all along the arm in the interval of galactocentric distances from 3–7 kpc. The negative sign of the mean azimuthal offset over spiral arm 1 from $R = 3$–7 kpc means that young populations of stars, surrounded by regions of ionized hydrogen, are located closer to the inner edge of spiral arm 1 within the SC–H II R pairs than relatively old star clusters without ionized gas. Does this mean that spiral arm 1 rotates more slowly than the matter in the disc over its entire extension? We will return to a discussion of this issue in Section 5.

Similar to the case of galaxy NGC 628, we investigated the behaviour of the first mode of the spiral density wave using the Fourier coefficients from the analysis of the velocity field. The radial variation of the criterion for the first mode (equation 5), calculated using Fourier coefficients derived from analysis of the velocity field of NGC 6946, shows that at distance $R = 4.4 \pm 1.0$ kpc the spiral pattern rotation velocity is equal to that of the disc (see bottom panel in Fig. 10). This means that the spiral patterns of the first and second modes of the spiral density wave in galaxy NGC 6946 rotate synchronously. It also means that the negative sign of the azimuthally averaged offset in 'heavy' arm 1 outside the corotation circle cannot be explained by the effect of the spiral shock wave, caused by the first and second modes.

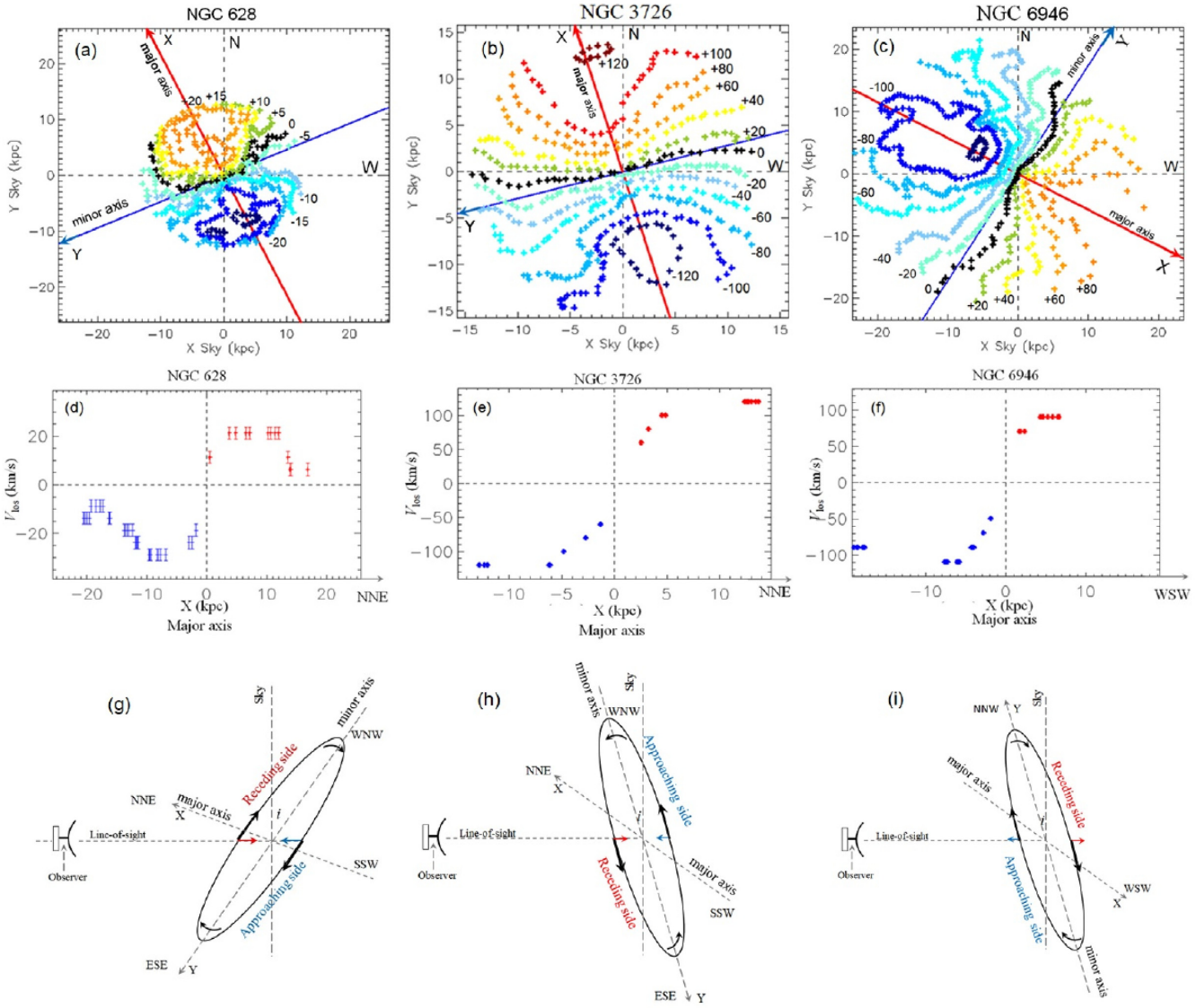

Figure 11. Fields of observed line-of-sight velocities V_{los} show receding and approaching sides of the galaxies studied (panels a–c). The velocity fields are based on observations published in Shostak & van der Kruit (1984), Verheijen & Sancisi (2001), Carignan et al. (1990). Panels (d)−(f) show observed V_{los} along the major axis. The V_{los} values are corrected for the systemic velocity of the galaxy but not for the inclination. The *x*-axis shown in this figure is aligned with the major axis of the galaxies studied and the *y*-axis coincides with the minor axis. The direction of the galaxy's major axis (*x*-axis) on the plane of the sky is shown in each panel. Panels (g)–(i) show the spatial orientation of the galaxies under study, determined from analysis of the azimuthal offset directions in the SC–H II R pairs and the observed velocity field.

4.4 The spatial orientation of the galaxies studied

Determining the spatial orientation (i.e. the nearest side to us) of a face-on galaxy with a low inclination using photometric measurements is difficult and ambiguous. One such galaxy is NGC 628, which we study in the current paper. Therefore, if one knows the direction of rotation in addition to the known approaching and receding sides, one can determine the nearest side of the galaxy. The sign of the mean azimuthal offset in thin ring zones and its variation as a function of galactocentric distance (see Sections 4.1, 4.2, and 4.3) determines the sense of rotation of matter in the discs of the galaxies studied: clockwise in the case of NGC 628 and NGC 6946, counterclockwise in the case of NGC 3726. The velocity field of NGC 628 presented in Fig. 11(a) shows that the north-north-east (NNE) part of the disc is the receding side and the south-south-east (SSW) part is the approaching side. The course of the observed velocities along the major axis of NGC 628, shown in Fig. 11(d), also shows that the north-north-east (NNE) side of the disc is moving away from the observer, while the south-south-west (SSW) side is moving closer to the observer. Fig. 11(g) shows that the east-south-east side (ESE) of NGC 628 is the nearest to us. The spatial orientations of galaxies NGC 3726 and NGC 6946 are defined similarly (see panels b, e, h for NGC 3726 and panels c, f, i for NGC 6946). Figs 11(h) and (i) show that the west-north-west side (WNW) of NGC 3726 and north-north-west side (NNW) of NGC 6946 are the nearest to us.

Fig. 12 plots the photometric profiles of the difference in mean surface brightness in the *B* band and the colour index $B - V$ between opposite sides from the centre along the minor axis in galaxies NGC

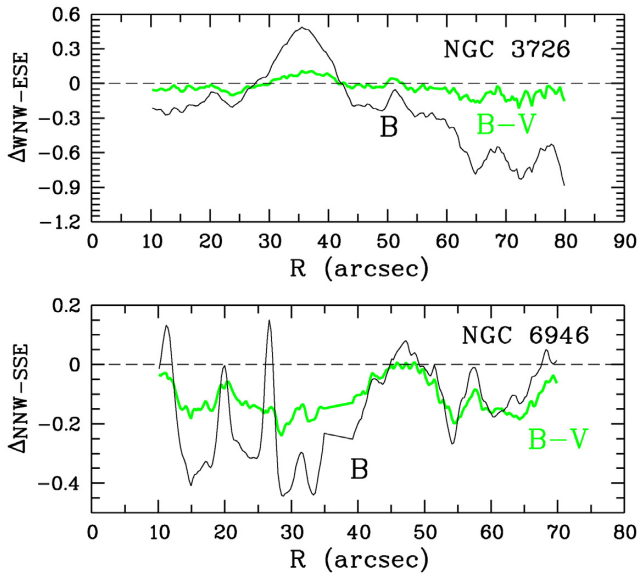

Figure 12. Top: Photometric profiles of the difference in mean surface brightness in the B band and the colour index $B - V$ between WNW and ESE parts of the minor axis in NGC 3726. Bottom: Photometric profiles of the difference in mean surface brightness in the B band and the colour index $B - V$ between NNW and SSE parts of the minor axis in NGC 6946. Averaging performed in a strip width of 1 arcmin. Deviations in positive values at $R =$ 30–40 arcsec for NGC 3726 are explained by the fact that the dust lane is located at these R values to the WNW, and part of the bright spiral arm is located in the ESE. The range of $R =$ 35–39 arcsec for NGC 6946 is ignored due to the bright field star at 37 arcsec to the south from the centre. See text for details.

3726 and NGC 6946, where

$$\Delta(B)_{\mathrm{WNW-ESE}}(R) = \mu(B)_{\mathrm{WNW}}(R) - \mu(B)_{\mathrm{ESE}}(R),$$
$$\Delta(B-V)_{\mathrm{WNW-ESE}}(R) = (B-V)_{\mathrm{WNW}}(R) - (B-V)_{\mathrm{ESE}}(R)$$

for NGC 3726,

$$\Delta(B)_{\mathrm{NNW-SSE}}(R) = \mu(B)_{\mathrm{NNW}}(R) - \mu(B)_{\mathrm{SSE}}(R),$$
$$\Delta(B-V)_{\mathrm{NNW-SSE}}(R) = (B-V)_{\mathrm{NNW}}(R) - (B-V)_{\mathrm{SSE}}(R)$$

for NGC 6946, and R is an apparent galactocentric distance. The photometric profiles in Fig. 12 also show that the nearest side of NGC 3726 is its west-north-west side (WNW), and the nearest side of NGC 6946 is its north-north-west side (NNW). The upper panel in Fig. 12 shows that the west-north-west (WNW) part of NGC 3726 in the B band is brighter and has a bluer colour index $B - V$. The lower panel in Fig. 12 shows that the north-north-west (NNW) part of NGC 6946 in the B band is brighter and has a bluer colour index $B - V$.

5 DISCUSSION

We now turn to a comparison of our results with estimates of corotation radii obtained by other methods. Table 2 summarizes the estimates of corotation radii in NGC 628, NGC 3726, and NGC 6946 obtained in the current study (columns 2 and 3) and compares them with results obtained by other methods (column 4).

5.1 NGC 628

Analysis of computer-enhanced images of galaxies NGC 628 revealed a three-arm structure along with a more pronounced two-arm structure (Elmegreen et al. 1992). The authors of this study interpreted the three-armed spiral ($m = 3$) as a result of the superposition of the first ($m = 1$) and second ($m = 2$) modes of the spiral density wave. According to this interpretation, the three-armed spiral is not an independent wave mode but a driven wave and a possible energy sink for the two-armed mode. The corotation radii determined from resonance fits of computer-enhanced images of galaxies NGC 628 (column 4 in Table 2) correspond (within the error interval) to the corotation resonances found from the velocity field of galaxies for the second ($m = 2$) mode of the spiral density wave (column 3 in Table 2). The other two methods by which the corotation radius in galaxy NGC 628 has been determined are based on analysing the radial change in relative star-formation efficiency (Cepa & Beckman 1990) and determining the galactocentric distance

Table 2. Summary of estimates of corotation radii in NGC 628, NGC 3726, and NGC 6946 obtained in this work (columns 2 and 3) in comparison with results obtained by other methods (column 4).

Galaxy	Method		
NGC	Azimuthal SF propagation (kpc)	Velocity field (kpc)	Other methods (kpc)
1	2	3	4
628	$R_{\mathrm{C,\,inner}} = 3.0 \pm 1.0$	$R_{\mathrm{C},\,m=1} = 3.0 \pm 1.0$	
	$R_{\mathrm{C,\,outer}} = 6.3 \pm 1.0^{i}$	$R_{\mathrm{C},\,m=2} = 6.2 \pm 1.0$	$R_{\mathrm{C}} \approx 5.0^{a}$
	$R_{\mathrm{C,\,outer}} = 7.0 \pm 1.0^{k}$		$R_{\mathrm{C}} = 5.2 \pm 1.3^{b}$
			$R_{\mathrm{C}} = 5.2 \pm 1.9^{c}$
3726	$R_{\mathrm{C1}} \approx 2$		$R_{\mathrm{C1}} = 1.8 \pm 0.2^{d}$
			$R_{\mathrm{C1}} = 2.5 \pm 0.2^{e}$
			$R_{\mathrm{C1}} = 1.5 \pm 0.1^{f}$
	$R_{\mathrm{C2}} = 4.4 \pm 1.0$	$R_{\mathrm{C},\,m=1} = 4.5 \pm 1.0$	$R_{\mathrm{C2}} = 4.4 \pm 0.2^{d}$
			$R_{\mathrm{C2}} = 4.2 \pm 0.2^{e}$
			$R_{\mathrm{C2}} = 4.5 \pm 0.2^{f}$
	$R_{\mathrm{C3}} = 9.8 \pm 1.0$	$R_{\mathrm{C},\,m=2} = 9.3 \pm 1.0$	$R_{\mathrm{C5}} = 9.9 \pm 0.2^{e}$
			$R_{\mathrm{C3}} \approx 8^{f}$
6946	$R_{\mathrm{C}} = 4.8 \pm 1.0$	$R_{\mathrm{C},\,m=1} = 4.4 \pm 1.0$	$R_{\mathrm{C}} \approx 4.4^{a}$
		$R_{\mathrm{C},\,m=2} = 4.4 \pm 1.0$	$R_{\mathrm{C}} = 4.7 \pm 1.2^{g}$
			$R_{\mathrm{C1}} = 3.2^{+0.6}_{-2.0}{}^{h}$
			$R_{\mathrm{C2}} = 8.8^{+0.4}_{-1.6}{}^{h}$
			$R_{\mathrm{C,\,spiral}} \approx 4.4^{i}$

Notes. The values of the corotation radius R_{C} found by other authors are rescaled according to R_{25} and the distances to the studied galaxies assumed in the current paper.
[a]Corotation radius R_{C} determined from the resonance fits of computer-enhanced galaxy images (Elmegreen et al. 1992).
[b]Corotation radius R_{C} determined from the analysis of the radial change in relative star-formation efficiency (Cepa & Beckman 1990).
[c]Corotation radius R_{C} determined from the galactic radii at which breaks or changes in the slope of the metallicity gradients occur (Scarano & Lepine 2013).
[d]From the Font–Beckman method, using the change in sense of the radial component of the in-plane velocity at a resonance radius (Font et al. 2011).
[e]From the Font–Beckman method, using the change in sense of the radial component of the in-plane velocity at a resonance radius (Font et al. 2014).
[f]Corotation radius R_{C} determined through the zero crossings of the radial distribution of phase shift (Buta & Zhang 2009).
[g]Corotation radius R_{C} determined from the pattern speed using the Tremaine–Weinberg method applied to the map of CO emission (Zimmer, Rand & McGraw 2004).
[h]Corotation radius R_{C} determined from the pattern speed using the Tremaine–Weinberg method applied to the H α velocity field (Fathi et al. 2007).
[i]Corotation radius R_{C} determined from the pattern speed using the Font–Beckman method applied to the H α velocity field (Font et al. 2019).
[j]Corotation radius R_{C} determined from the radial change in azimuthally averaged offset in the annulus calculated for all 503 SC–H II R pairs in NGC 628.
[k]Corotation radius R_{C} determined from the radial change in azimuthally averaged offset in the annulus calculated for 324 SC–H II R pairs outside the peculiar spiral A in NGC 628.

at which breaks or changes in the slope of the metallicity gradients occur (Scarano & Lepine 2013).

Smaller values of corotation radius $R_C \approx 5$ kpc obtained by other methods (column 4 in Table 2) for NGC 628 in comparison with our evaluation $R_C \approx 7$ kpc (column 2) can be explained by the following: the latter was obtained for 324 SC–H II R pairs outside the peculiar spiral A. Fig. 4(a) shows that the radial variation of the mean azimuthal offset calculated for all 503 SC–H II R pairs, including those from spiral arm A, yields a corotation radius $R_C = 6.3 \pm 1.0$ kpc, closer to the estimates of other authors. The estimates of the corotation radius in the papers cited in Table 2 did not take into account the peculiarity of spiral arm A of NGC 628.

Recall briefly how the star-forming regions in spiral arm A of galaxy NGC 628 differ from the others. Gusev et al. (2014) show that the star-forming regions in spiral arm A are systematically brighter in the UV and in the Hα line, larger in size, higher in star-formation rate, lower in metallicity, and relatively lower in age than the brightest star-forming regions in other arms. The larger sizes and masses/luminosities are determined by the parameters of the interstellar medium, such as gas density and pressure (Elmegreen & Efremov 1997; Kennicutt 1998; Billett, Hunter & Elmegreen 2002; Larsen 2002). High gas densities and pressures are provided by a more intense spiral shock wave. The intensity of the spiral shock wave depends on the difference between the rotational velocities of the matter in the disc and the spiral pattern.The positive sign of the mean azimuthal offset along the entire length of spiral arm A (see Fig. 4b) indicates that the rotation speed of spiral arm A is everywhere higher than the rotation speed of the substance in the disc. Spiral A relates to the asymmetric structure detected by Elmegreen et al. (1992) using a computer-enhanced image of the galaxy NGC 628. The bottom panel in Fig. 5 shows that the rotation rate of the first asymmetric mode ($m = 1$) is higher than that of the matter in the disc from about 3 kpc onwards, where the rotation curve of galaxy NGC 628 enters a plateau. Therefore, the difference between the disc speed and the speed of the asymmetric spiral pattern of the first mode ($m = 1$) grows faster than the difference between the disc speed and the speed of the symmetric spiral pattern of the second mode ($m = 2$). Thus, a higher gas density and pressure at the outer edge of spiral arm A can be achieved compared to the gas density and pressure at the inner edge of symmetrical spiral arms. This conclusion agrees well with the result by Elmegreen & Elmegreen (1983), who found that only arm A of NGC 628 has regular chains of the brightest star-forming complexes.

The area inside the corotation radius ($R_{C,\,m=1} = 3 \pm 1$ kpc) of the first mode ($m = 1$) coincides with the region of influence of the bar-like structure that forms a circular ring of gas clouds from which a circumnuclear ring of star formation emerges (Combes & Gerin 1985). Perhaps that is why the sign of the azimuthal offset in arm A also remains positive inside the corotation circle of the first mode, where star-formation processes are determined by the bar potential, including the circumnuclear ring of star formation detected in the infrared (Seigar 2002).

In Section 1, we noted that the search for a displacement in the azimuthal distribution of the three investigated samples of star clusters of different ages in galaxy NGC 628 did not yield a positive result (Shabani et al. 2018). In the current study the azimuthal component of the spatial offset is determined between a young star cluster and the nearest H II region within the same star-formation complex. Shabani et al. (2018) have determined the azimuthal gradient of ages by comparing the angular offset of the positions of the statistical peaks of samples of young (age <10 Myr) and intermediate-age star clusters (10 < age < 50 Myr) from the ridge of the spiral arm, and the angular offset of the statistical peaks of a sample of old star clusters (50 < age < 200 Myr) from this ridge. Thus, this approach implies that the age of the star cluster should correlate with the angular offset of the cluster from the ridge of the spiral arm. Gusev & Shimanovskaya (2019) showed that, unlike the spiral structure, turbulence and the stochastic self-propagating star-formation wave (SSPSF) are the dominant mechanisms in the galaxies that they studied, including NGC 628. However, this does not exclude the contribution of spiral shock to star formation, which manifests itself as an azimuthal component of the spatial offset between an extremely young stellar population and an intermediate-age population in a young star-formation complex. When the SSPSF mechanism dominates, the spatial offset between clusters of different ages is determined by the speed and direction of the self-propagating wave. If stochastic star formation does not propagate across, but predominantly along, the spiral arm, then older clusters may crowd closer to the ridge of the spiral arm than relatively young clusters spawned by a wave propagating in the other direction. That is, if the SSPSF mechanism dominates, the correlation between age and angular offset of the cluster from the ridge of the spiral arm will be broken.

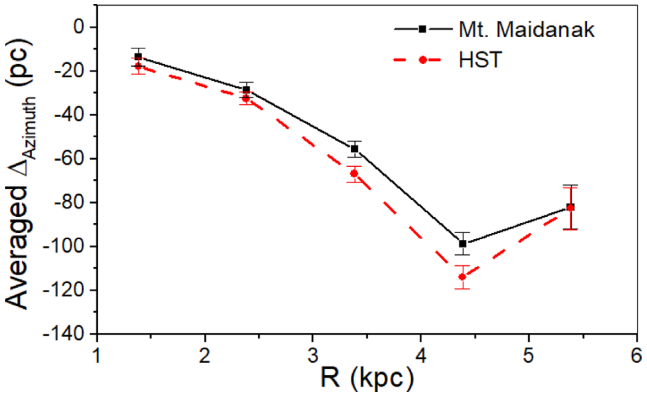

Figure 13. Comparison between the radial change of the azimuthally averaged offset in the annulus calculated for 62 reference pairs SC–H II R observed by *HST* (red dashed line) and the radial change calculated for 62 pairs from our sample (black solid line) identified with *HST* objects.

In Fig. 13 we compare a radial change of the azimuthally averaged offset in the annulus calculated for 62 reference pairs SC–H II R observed by *HST* (red dashed line) with a radial change calculated for 62 pairs from our sample (black solid line) identified with *HST* objects. Fig. 13 demonstrates a good agreement, within the error intervals, between the radial variation of the averaged azimuthal offset in the thin annulus derived from the highly accurate *HST* data and the radial variation derived from our ground-based imaging data.

5.2 NGC 3726

For the barred galaxy NGC 3726, we have found three estimates of the corotation radius, confirming earlier results by Buta & Zhang (2009) with the potential-density phase-shift method and by Font et al. (2011, 2014) with the Font–Beckman method for finding dynamical resonances in disc galaxies, using the change in direction of the radial component of the residual velocity at the resonance radius. All estimates of the innermost resonance, including the result of the current study, lie in the range of galactocentric distances from 1.5–2.5 kpc in the area occupied by the bar, which is outside the scope of the present paper.

Two of the three corotation radii lie well outside the bar ends. The intermediate corotation radius $R_{C2} = 4.4 \pm 1.0$ kpc found at galactocentric distance, where the azimuthally averaged offset changes sign from negative to positive (Fig. 6), is confirmed by the corotation radius found for the first mode ($m = 1$) of the spiral density wave (Table 2, column 3) and agrees with the estimates $R_{C2} = 4.5 \pm 0.2$ kpc given by the potential-density phase-shift method (Buta & Zhang 2009), and $R_{C2} = 4.4 \pm 0.2$ kpc (Font et al. 2011) and $R_{C2} = 4.2 \pm 0.2$ kpc (Font et al. 2014) given by the Font–Beckman method using the change of sense of the radial component of the residual velocity at the resonance radius.

According to the theoretical calculations of Contopoulos (1980) and numerical simulations of Athanassoula (1992) and Garma-Oehmichen et al. (2021), which were confirmed observationally by Font et al. (2014), for 32 barred galaxies, the bar corotation occurs not far from the end of the bar. The value of the ratio between the corotation radius and the bar length $\mathcal{R} \approx 1.38$ calculated for NGC 3726 using R_{C2} from column 2 of Table 2 and the bar length $R_{bar} \approx 3.2$ kpc as reported by Eskridge et al. (2002) is compatible with $\mathcal{R} = 1.30 \pm 0.05$ for this galaxy and agrees with the average value of this ratio $\mathcal{R} = 1.35 \pm 0.36$ kpc obtained by Font et al. (2014). It is interesting to note that this intermediate resonance at galactocentric distance $R \approx 4.5$ kpc is also detected by us in Fig. 7 (bottom panel), which shows the radial change of a quantity proportional to the difference between the angular speed of the spiral pattern and the angular speed of matter in the disc (see criterion 5), calculated using Fourier coefficients obtained from velocity field analysis of galaxy NGC 3726 for the first mode ($m = 1$) of the spiral density wave. This means that the first mode ($m = 1$) of the spiral density wave in NGC 3726 shares a rotation speed with the bar and is probably induced by the bar.

The estimation of the outer corotation radius $R_{C3} \approx 8$ kpc by Buta & Zhang (2009), as noted by the authors themselves, is less confident than the estimate of $R_{C2} = 4.5 \pm 0.2$ kpc. Font et al. (2011, 2014) found two other resonances at galactocentric distances $R_{C3} \approx 7$ kpc and $R_{C4} \approx 8.5$ kpc. One of them ($R_{C3} \approx 7$ kpc) does not coincide with any of the resonances found in the current study using the azimuthal offset and in the work by Buta & Zhang (2009) using the potential-density phase-shift method, while R_{C4} at 8.5 kpc is compatible with $R_{C3} \approx 8$ kpc according to Buta & Zhang (2009).

The outer resonance $R_{C5} = 9.9 \pm 0.2$ kpc obtained by Font et al. (2014) can be associated with the corotation radius obtained from the azimuthal offset (column 2 in Table 2) and the corotation radius obtained for the second mode of the spiral density wave (column 3 in Table 2).

5.3 NGC 6946

In the case of NGC 6946, a comparison of our results (columns 2 and 3 in Table 2) with the estimates of the corotation radius (column 4 in Table 2) obtained from the resonance fits of computer-enhanced galaxy images (Elmegreen et al. 1992) and from the pattern speed using the Tremaine–Weinberg method, applied to the map of CO emission (Zimmer et al. 2004) and the Hα velocity field (Fathi et al. 2007), gives a satisfactory agreement for these estimates within the error intervals. The radii of the corotation resonances obtained in Fathi et al. (2007) have been read (and rescaled) by us from Fig. 5 of this paper, where the radial change of angular frequency of the gas in disc is compared with the pattern speeds derived for the inner and outer regions of the disc. Note also that the estimate of the corotation radius $R_{C,\,spiral} \approx 4.4$ kpc for NGC 6946 calculated using the spiral pattern speed from Font et al. (2019) is compatible with the results of the current study. The second corotation radius $R_{C2} \approx 8.8$ kpc, found by Fathi et al. (2007), may explain the slower rotation of the 'heavy' arm 1 in NGC 6946 and thus the negative sign of the azimuthally averaged offset along the entire length of this peculiar arm. This observational result confirms the multiple-bar structure discussed in Fathi et al. (2007), in which the bars have different pattern speeds.

6 CONCLUSION

Analysis of the spatial displacement between H II regions and young clusters allowed us to determine an important parameter of the theory of the spiral structure of galaxies, namely the location of the corotation radius in nearby spiral galaxies: NGC 628, NGC 3726, and NGC 6946. Fourier analysis of the velocity field carried out in the same galaxies provided independent determination of the corotation resonance positions, which are in agreement with the estimates obtained from azimuthal age-gradient analysis in young star-formation complexes.

We found a correlation between features of radial change of averaged azimuthal offset in SC–H IIR pairs and two coupled modes of the spiral density wave revealed by Fourier analysis of the H I velocity field in target galaxies. This finding is consistent with the multiresonance structure confidently detected by the Font–Beckman method in 79 spirals and the paradigm of multiple coupled spiral patterns (Font et al. 2011, 2014, 2019).

The behaviour of the mean azimuthal offset in the peculiar arms in NGC 628 (spiral A) and NGC 6946 (heavy spiral 1) shows that spiral A rotates faster than the matter in the disc of NGC 628 and 'heavy' spiral 1 rotates more slowly than the matter in the disc of NGC 6946. In the spiral shock-induced star-formation scenario, this suggests that spiral A in NGC 628 is driven by the first mode of the spiral density wave, and 'heavy' spiral 1 in NGC 6946 is driven by the slowly rotating so-called large-scale oval diagnosed in Fathi et al. (2007). This means that more than one density-wave mode can coexist in the region of the spiral structure, each rotating at its own pattern speed.

In the bar galaxy NGC 3726 we have identified three corotational radii detected by the radial change of the averaged azimuthal offset in SC–H IIR pairs with the corotational radii detected by Font et al. (2011, 2014) using the Font–Beckman method applied to the Hα velocity field, thereby confirming the multiresonance structure in this galaxy. Identification of two of the four outer resonances found by Font et al. (2011, 2014) with galactocentric distances at which the averaged azimuthal offset in SC–H IIR pairs changes sign links these resonances to morphological features of the spiral structure of NGC 3726. The coincidence of the corotation radii of the bar and the first mode of the spiral density wave in NGC 3726 may be an observational indication that the first mode is induced by the bar.

Clockwise rotation in the Z-shaped galaxies NGC 628 and NGC 6946 and counterclockwise rotation in the S-shaped galaxy NGC 3726, determined by a radial change of sign of mean azimuthal offset in thin ring zones, classify the studied galaxies as trailing spirals, the type to which most spiral galaxies belong. Knowing the sense of rotation and the approaching/receding sides of the galaxy made it possible to determine the spatial orientation (i.e. the nearest side to us) of NGC 628, for which the usual definition by photometric measurements gives a dubious result. The application of this method to the other two galaxies studied confirmed the results obtained from the photometric measurements.

Our detailed analysis of the azimuthal offset between stellar populations of different ages in pairs carried out in morphologically different spiral galaxies, namely in the multiple-arm spiral galaxy

NGC 628 with a strongly pronounced 'peculiar arm A' (Gusev et al. 2014), in galaxy NGC 3726 with a strongly pronounced bar (Eskridge et al. 2002), and in spiral galaxy NGC 6946 with one heavy arm, according to Arp's classification (Arp 1966), confirm the prediction of one of the main theories explaining spiral formation in galaxies by a stationary spiral density wave.

ACKNOWLEDGEMENTS

We are very grateful to the referee for their comments, which greatly improved the current article. Photometric observations for this article were taken at the 1.5 m telescope of the Mt Maidanak Observatory in Uzbekistan. The authors acknowledge the usage of the Barbara A. Miculski archive for space telescopes (http://archive.stsci.edu). This study was partly supported by the Russian Foundation for Basic Research (project no. 20-02-00080) and conducted within the framework of an agreement on academic cooperation and exchange between the University of Applied Sciences of Mittelhessen, Germany and the Sternberg Astronomical Institute of Lomonosov Moscow State University, Russia.

DATA AVAILABILITY

The LEGUS public access data used in this article are available in the Barbara A. Miculski archive for space telescopes at http://archive.stsci.edu/prepds/legus/dataproducts-public.html. The CFHT data have been published as supplementary data at https://academic.oup.com/mnras/article/477/3/4152/. Our data can be shared on request to the corresponding author.

REFERENCES

Adamo A. et al., 2017, ApJ, 841, 131
Arp H., 1966, Atlas of Peculiar Galaxies. California Institute of Technology Publ., Pasadena
Athanassoula E., 1992, MNRAS, 259, 328
Berdnikov L. N., 1987, SvA Lett., 13, 45
Billett O. H., Hunter D. A., Elmegreen B. G., 2002, AJ, 123, 1454
Bonnarel F., Boulesteix J., Georgelin Y. P., Lecoarer E., Marcelin M., Bacon R., Monnet G., 1988, A&A, 189, 59
Buta R. J., Zhang X., 2009, ApJS, 182, 559
Canzian B., 1993, ApJ, 414, 487
Canzian B., Allen R. J., 1997, ApJ, 479, 723
Carignan C., Charbonneaur P., Boulanger F., Viallefond F., 1990, A&A, 234, 43
Cepa J., Beckman J., 1990, ApJ, 349, 497
Combes F., Gerin M., 1985, A&A, 150, 327
Contopoulos G., 1980, A&A, 81, 198
Efremov Y. N., 1985, SvA Lett., 11, 69
Elmegreen B. G., Efremov Y. N., 1997, ApJ, 480, 235
Elmegreen B. G., Elmegreen D. M., 1983, MNRAS, 203, 31
Elmegreen B. G., Elmegreen D. M., Montenegro L., 1992, ApJS, 79, 37
Eskridge P. B. et al., 2002, ApJS, 143, 73
Fathi K., Toonen S., Falcon-Barroso J., Beckman J., Hernandez O., Daigle O., Carignan C., de Zeeuw T., 2007, ApJ, 667, L137
Font J., Beckman J. E., Epinat B., Fathi K., Gutierrez L., Hernandez O., 2011, ApJ, 741, L14
Font J., Beckman J. E., Querejeta M., Epinat B., James P. A., Blasco-Herrera J., Erroz-Ferrer S., Pérez I., 2014, ApJS, 210, 2
Font J., Beckman J. E., James Ph. A., Patsis P. A., 2019, MNRAS, 482, 5362
Fridman A. M. et al., 2001a, MNRAS, 323, 651
Fridman A. M. et al., 2001b, A&A, 371, 538
Garma-Oehmichen L., Martinez-Medina L., Hernandez-Toledo H., Puerari I., 2021, MNRAS, 572, 4708
Guidoni U., Messi R., Natali G., 1981, A&A, 96, 215
Gusev A. S., Shimanovskaya E. V., 2019, MNRAS, 488, 3045
Gusev A. S., Egorov O. V., Sakhibov F., 2014, MNRAS, 437, 1337
Gusev A. S., Guslyakova S. A., Novikova A. P., Khramtsova M. S., Bruevich V. V., Ezhkova O. V., 2015, Astron. Rep., 59, 899
Gusev A. S. et al., 2016, MNRAS, 457, 3334
Gusev A. S., Shimanovskaya E. V., Shatsky N. I., Sakhibov F., Piskunov A. E., Kharchenko N. V., 2018, Open Astron., 27, 98
Henize K. G., 1956, ApJS, 2, 315
Kamphuis J., Briggs F., 1992, A&A, 253, 335
Kennicutt R. C., 1998, ApJ, 498, 541
Larsen S. S., 2002, AJ, 124, 1393
Oye M. S., Parker J. S., Mikles V., Zhang X., 2003, AJ, 126, 2317
Pavlovskaya E. D., Suchkov A. A., 1984, SvA, 28, 389
Pikel'ner S. B., 1971, SvA, 14, 602
Puerari I., Dottori H., 1997, ApJ, 476, L73
Roberts W. W., 1969, ApJ, 158, 123
Rogstad D. H., Shostak G. S., 1973, A&A, 22, 111
Rousseau-Nepton L., Robert C., Martin R. P., Drissen L., Martin T., 2018, MNRAS, 477, 4152
Sakhibov F. K., Smirnov M. A., 1987, SvA, 31, 132
Sakhibov F. K., Smirnov M. A., 1989, SvA, 33, 476
Sakhibov F. K., Smirnov M. A., 1990, SvA, 34, 347
Sakhibov F., Zinchenko I. A., Pilyugin L. S., Grebel E. K., Just A., Vílchez J. M., 2018, MNRAS, 474, 1657
Sanchez S. F., Rosales-Ortega F. F., Kennicutt R. C., Johnson B. D., Diaz A. I., Pasquali A., Hao C. N., 2011, MNRAS, 410, 313
Scarano S., Jr, Lepine J. R. D., 2013, MNRAS, 428, 625
Seiden P. E.,1985, in Van Woerden H., Allen R. J., Butler B. W., eds, Proc. IAU Symp. 106, The Milky Way Galaxy. D. Reidel Publishing Co., Dordrecht, p. 551
Schweizer F., 1976, ApJS, 31, 313
Seigar M. S., 2002, A&A, 393, 499
Shabani F. et al., 2018, MNRAS, 478, 3590
Shostak G. S., van der Kruit P. C., 1984, A&A, 132, 20
Shu F. H., Yuan C., Goldsmith D. W., Roberts W. W., 1972, ApJ, 173, 557
Shu F. H., Milione V., Roberts W. W., 1973, ApJ, 183, 819
Sierra A. D., Seigar M. S., Treuthardt P., Puerari I., 2015, MNRAS, 450, 1799
Smirnov M. A., Sakhibov F., 1981, Akademiia Nauk Tadzhikskoi SSR, Doklady, 24, 725
Talbot J. R., Jensen E. B., Dufour R. J., 1979, ApJ, 229, 91
Vallée J. P., 2019, MNRAS, 489, 2819
Verheijen M. A., Sancisi R., 2001, A&A, 370, 765
Zimmer P., Rand R. G., McGraw J. T., 2004, ApJ, 607, 285
Zinchenko I. A. et al., 2019, A&A, 628, A55

This paper has been typeset from a TEX/LATEX file prepared by the author.